

Double Closed-loop Control Scheme of Yaw Rate for Active Front Steering System

JIANWEI WEI^{1,2} WANZHONG ZHAO² WEIYAN SHANG¹

¹School of Mechanical Engineering, Ningbo University of Technology
Cuibai St., Ningbo 315016

²College of Energy and Power Engineering, Nanjing University of Aeronautics and Astronautics
Yudao St., Nanjing 210016
jianweinb@163.com

Abstract: - Steering system is an important man-machine interface, for which transmits driver's lateral control intention to the vehicle. In order to improve the vehicle lateral stability, a double closed-loop control scheme of yaw rate for active front steering system was proposed in this paper. To investigate the control effects of the double closed-loop control scheme of yaw rate, a two degree-of-freedom (2DOF) vehicle model and brushless dc motor (BLDCM) model were built, as well as numerical simulations and virtual tests based on CarSim software were conducted at different limiting conditions. Results indicate that response delay of vehicle driving on the road with low adhesion coefficient could be reduced with the help of the proposed yaw rate control scheme, as well as effects of unexpected yaw disturbance on response characteristics of vehicle could be weakened effectively.

Key-Words: - Vehicle, active front steering, yaw rate control, brushless dc motor (BLDCM), double closed-loop control, CarSim

1 Introduction

Lateral stability is considered one of the most important aspects of vehicle active safety, while vehicle is running at limiting conditions. It is noteworthy that steering system is an important man-machine interface, for which transmits driver's lateral control intention to the vehicle. Since BMW AG has developed its active front steering system (AFS), more attention is paid for that active front steering control system, for which can increase ride comfort and active safety. Furthermore, existing research results indicate that a greater vehicle controllability and lateral stability could be achieved by active front steering control than by four-wheel steering (4WS) system or direct yaw-moment control (DYC) system especially for full braking testing on a μ - split road and slalom testing on packed snow[1].

At present, a number of studies are focused on yaw rate control for active steering system. The research emphasis are on the decision control of yaw rate[2][3], as well as the applying of advanced control theories to the yaw rate control[4]. However, problem of the control accuracy of the actuator motor for active front steering has been forgotten.

The aim of this paper is to investigate a double closed-loop control scheme of yaw rate, one closed-loop is used for angular displacement tracking control, and the other closed-loop is used for decision control of yaw rate. By double closed-loop control of yaw rate, response delay of vehicle driving on the road with low adhesion coefficient can be reduced, as well as effects of unexpected yaw disturbance on response characteristics of vehicle could be weakened effectively.

The rest of this paper is organized as follows: in section 2, two-degree-of-freedom (2DOF) vehicle model, brushless dc motor (BLDCM) model, and side wind model are described briefly. Section 3 describes the double closed-loop control scheme, as well as the angular displacement tracking controller and decision controller of yaw rate were designed. In section 4, a serious numerical simulation of limiting condition were carried out, and followed by virtual tests based on CarSim software in section 5. Conclusions are presented in 6.

2 Modeling

2.1 Vehicle Model

In this paper, assuming steering angle and side slip angle to be small, then the 2DOF vehicle model can

be derived, which is shown in Fig.1. And, the lateral translation and rotational yaw motion equations written in the vehicle fixed frame take the following form[5][6].

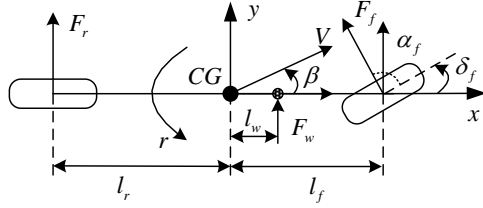


Fig.1 2DOF vehicle model

$$\begin{bmatrix} mV(\dot{\beta} + r) \\ I_z \dot{r} \end{bmatrix} = \begin{bmatrix} F_f + F_r + F_w \\ F_f l_f - F_r l_r + F_w l_w \end{bmatrix} \quad (1)$$

$$\begin{cases} F_f(\alpha_f) = \mu K_f \alpha_f \\ F_r(\alpha_r) = \mu K_r \alpha_r \end{cases} \quad (2)$$

$$\delta_f = \frac{1}{G} \theta'_p = \frac{1}{G} (\theta_{sw} + \theta_{ac}) \quad (3)$$

$$\begin{cases} \alpha_f = \delta_f - (\beta + \frac{l_f}{V} r) \\ \alpha_r = -(\beta - \frac{l_r}{V} r) \end{cases} \quad (4)$$

Here, m represents total mass of the vehicle; l_f and l_r are distance between centre of gravity (CG) and the front and rear axle; F_f and F_r represent the front and rear tire force. r and β are the yaw rate and chassis side slip angle at centre of gravity; F_w represents a wind force acting at the aero dynamical center of the side surface at a distance l_w , from the center of gravity; I_z is the moment of inertia with respect to a vertical axis through the CG, and V is the magnitude of velocity vector at CG; α_f and α_r represent side slip angle of the front and rear tire; μ is the road adhesion factor; K_f and K_r represent the tire cornering stiffness; δ_f is the front wheel steering angle.

Then, the state space equation of the 2DOF vehicle model is:

$$\begin{cases} \dot{\hat{x}} = \hat{A}\hat{x} + \hat{B}u + B_w F_w \\ \hat{y} = \hat{C}\hat{x} \end{cases} \quad (5)$$

where,

$$\hat{x} = [r, \beta]; \hat{A} = \begin{bmatrix} a_{21} & a_{22} \\ a_{11} & a_{12} \end{bmatrix}; \hat{B} = \begin{bmatrix} b_2 \\ b_1 \end{bmatrix};$$

$$B_w = \begin{bmatrix} l_w / I_z \\ 1 / (mV) \end{bmatrix}; \hat{C} = \begin{bmatrix} 1 & 0 \\ 0 & 1 \end{bmatrix};$$

$$a_{11} = -\mu(K_f + K_r) / (mV);$$

$$a_{12} = -1 - \mu(K_f l_f - K_r l_r) / (mV^2);$$

$$a_{21} = -\mu(K_f l_f - K_r l_r) / I_z;$$

$$a_{22} = -\mu(K_f l_f^2 + K_r l_r^2) / (I_z V);$$

$$b_1 = \mu K_f / (mV);$$

$$b_2 = \mu K_f l_f / I_z.$$

2.2 BLDCM Model

In this paper, brushless dc motor (BLDCM) was used as the actuator motor for active front steering, and equivalent circuit model of the BLDCM is shown in Fig.2[7].

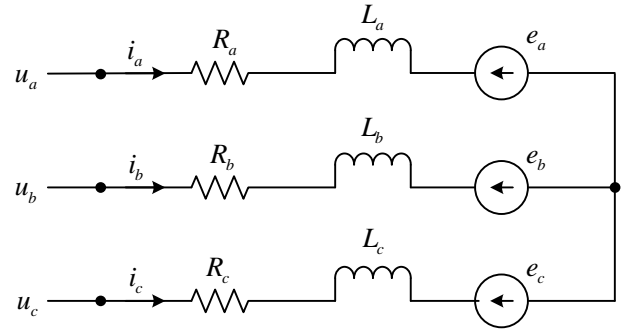


Fig.2 Equivalent circuit model of the BLDCM

Applying Kirchhoff's voltage law for the three phase stator loop winding circuits yields

$$\begin{aligned} u_a &= R_a i_a + L_a \frac{di_a}{dt} + M_{ab} \frac{di_b}{dt} + M_{ac} \frac{di_c}{dt} + e_a \\ u_b &= R_b i_b + L_b \frac{di_b}{dt} + M_{ba} \frac{di_a}{dt} + M_{bc} \frac{di_c}{dt} + e_b \\ u_c &= R_c i_c + L_c \frac{di_c}{dt} + M_{ca} \frac{di_a}{dt} + M_{cb} \frac{di_b}{dt} + e_c \end{aligned} \quad (6)$$

Here, u_a, u_b and u_c are phase voltages; e_a, e_b and e_c represent the back-EMF waveforms, which are functions of angular velocity of the rotor shaft; i_a, i_b and i_c are phase currents; R_a, R_b and R_c represent the phase resistances; L_a, L_b and L_c are stator self inductances; $M_{ab}, M_{ac}, M_{ba}, M_{bc}, M_{ca}$ and M_{cb} represent the mutual inductances.

The BLDCM mathematical model can be represented by the following equation in matrix form

$$\begin{bmatrix} L_a & M_{ab} & M_{ac} \\ M_{ba} & L_b & M_{bc} \\ M_{ca} & M_{cb} & L_c \end{bmatrix} \frac{d}{dt} \begin{bmatrix} i_a \\ i_b \\ i_c \end{bmatrix} = \begin{bmatrix} u_a \\ u_b \\ u_c \end{bmatrix} - \begin{bmatrix} R_a & 0 & 0 \\ 0 & R_b & 0 \\ 0 & 0 & R_c \end{bmatrix} \begin{bmatrix} i_a \\ i_b \\ i_c \end{bmatrix} - \begin{bmatrix} e_a \\ e_b \\ e_c \end{bmatrix} \quad (7)$$

Assuming the rotor has a surface-mounted design, and no saliency such that the stator self inductances are independent of the rotor position[7], hence

$$L_a = L_b = L_c = L \quad (8)$$

And, the mutual inductances will have the form

$$\begin{aligned} M_{ab} = M_{ac} = M_{ba} \\ = M_{bc} = M_{ca} = M_{cb} = M \end{aligned} \quad (9)$$

Assuming three phase balanced system, all the phase resistances are equal, then

$$R_a = R_b = R_c = R \quad (10)$$

Thus, equation (7) can be rewritten as

$$\begin{bmatrix} L & M & M \\ M & L & M \\ M & M & L \end{bmatrix} \frac{d}{dt} \begin{bmatrix} i_a \\ i_b \\ i_c \end{bmatrix} = \begin{bmatrix} u_a \\ u_b \\ u_c \end{bmatrix} - \begin{bmatrix} R & 0 & 0 \\ 0 & R & 0 \\ 0 & 0 & R \end{bmatrix} \begin{bmatrix} i_a \\ i_b \\ i_c \end{bmatrix} - \begin{bmatrix} e_a \\ e_b \\ e_c \end{bmatrix} \quad (11)$$

For the star type conjunction on three-phase winding is adopted, holds[8]

$$i_a + i_b + i_c = 0 \quad (12)$$

$$M i_b + M i_c = -M i_a \quad (13)$$

Then, equation (11) can be replaced by

$$\begin{bmatrix} L-M & 0 & 0 \\ 0 & L-M & 0 \\ 0 & 0 & L-M \end{bmatrix} \frac{d}{dt} \begin{bmatrix} i_a \\ i_b \\ i_c \end{bmatrix} = \begin{bmatrix} u_a \\ u_b \\ u_c \end{bmatrix} - \begin{bmatrix} R & 0 & 0 \\ 0 & R & 0 \\ 0 & 0 & R \end{bmatrix} \begin{bmatrix} i_a \\ i_b \\ i_c \end{bmatrix} - \begin{bmatrix} e_a \\ e_b \\ e_c \end{bmatrix} \quad (14)$$

Since the electromagnetic torque for this three-phase BLDCM is dependent on the current, speed and back-EMF waveforms, the instantaneous electromagnetic torque can be represented as

$$T_{ac} = \frac{1}{\omega_{ac}} (e_a i_a + e_b i_b + e_c i_c) \quad (15)$$

For the speed of the BLDC motor can be controlled by means of a three-phase and half-bridge pulse-width modulation (PWM) inverter, then the dynamic characteristic equations of BLDCM can be represented as[9]

$$U = E + R_{equ} i_{equ} + L_{equ} \frac{di_{equ}}{dt} \quad (16)$$

$$E = K_{eac} \omega_{ac} \quad (17)$$

$$\begin{aligned} T_{ac} &= \frac{1}{\omega_{ac}} E i_{equ} = K_{Tac} i_{equ} \\ &= J_{ac} \dot{\omega}_{ac} + B_{ac} \omega_{ac} + T_L \end{aligned} \quad (18)$$

where, U is the applied voltage; ω_{ac} is the motor speed; L_{equ} is the inductance of the stator; i_{equ} is the current of the circuit; R_{equ} is the resistance of the stator; E is the back electromotive force; T_{ac} is the torque of motor; T_L is the load torque; B_{ac} is the viscous coefficient; J_{ac} is the moment of inertia; K_{Tac} is the motor torque constant; K_{eac} is the back electromotive force constant.

2.3 Side Wind Model

In this paper, a wind model proposed by National Aeronautics and Space Administration (NASA) was used to simulate the driving environment with the disturbance of side wind. The transfer function of the side wind is of the fourth order and was obtained by Gawronski and Mellstrom[10][11]

$$H(s) = \frac{a_3 s^3 + a_2 s^2 + a_1 s + a_0}{b_4 s^4 + b_3 s^3 + b_2 s^2 + b_1 s + b_0} \quad (19)$$

Here, s is the Laplacian operator, $a_0 = 3.42$, $a_1 = 686.3$, $a_2 = 230.1$, $a_3 = 3.902$, $b_0 = 0.354$, $b_1 = 22.78$, $b_2 = 224.7$, $b_3 = 38.3$, $b_4 = 0.331$.

For vehicle dynamics applications, since gusts with frequencies greater than 2 Hz are not interested, an additional filter was added to limit the gust variations to within the frequency band of automotive chassis response. The transfer function of the additional filter can be given by[10]

$$F(s) = \frac{1}{s+1} \quad (20)$$

3 Double Closed-loop Control Scheme

To reduce the time lag of the steering system, which accounts for 60 percent of the total time lag[12], control accuracy of the actuator motor for active front steering appears especially important. Thus, a double closed-loop control scheme of yaw rate for active front steering is introduced, which is shown in Fig.3.

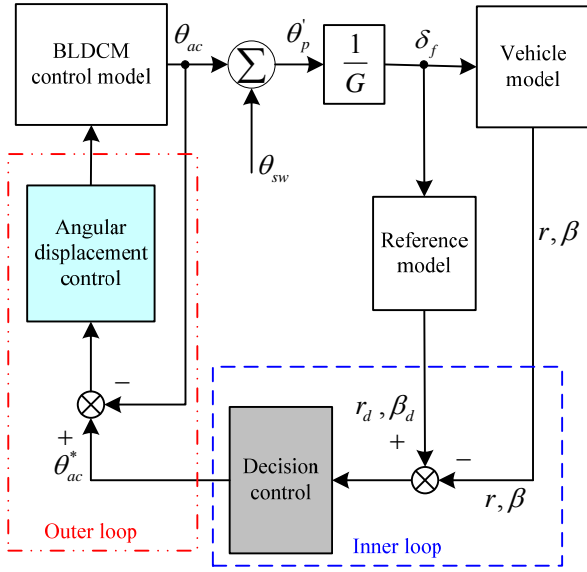


Fig.3 Double closed-loop control scheme.

Referring to Fig.3, the inner closed-loop is used for angular displacement tracking control, and the outer closed-loop is used for decision control of yaw rate.

3.1 Angular Displacement Tracking Control

Based on the characteristic equations of the BLDCM model, the open-loop transfer function $G_{U\theta}(s)$ from the applied voltage to the angular displacement has the form

$$G_{U\theta}(s) = \frac{K_{Tac}}{K_{Tac}K_{eac}s + s(L_{equ}s + R_{equ})(J_{ac}s + B_{ac})} \quad (21)$$

The controller $C(s)$ was chosen to be a PID controller, and the transfer function is

$$C(s) = K_p + \frac{K_i}{s} + K_d s \quad (22)$$

Then, construction of the closed loop system could be shown in Fig.4.

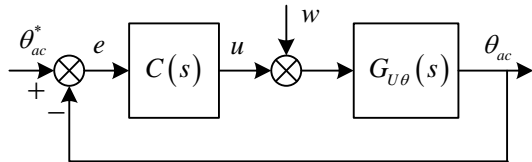


Fig.4 The angular displacement tracking control.

Then, the transfer function $G_{U\theta}(s)$ is converted into observable state space system and given by the model as[13]

$$\begin{cases} \dot{x} = Ax + B(u + w) \\ y = Cx \end{cases} \quad (23)$$

Here,

$$A = \begin{bmatrix} 0 & 0 & 0 \\ 1 & 0 & -\frac{B_{ac}R_{equ} + K_{Tac}K_{eac}}{J_{ac}L_{equ}} \\ 0 & 1 & -a_{33} \end{bmatrix};$$

$$B = \begin{bmatrix} \frac{K_{Tac}}{J_{ac}L_{equ}} \\ 0 \\ 0 \end{bmatrix};$$

$$C = [0 \quad 0 \quad 1];$$

$$a_{33} = \frac{J_{ac}R_{equ} + B_{ac}L_{equ}}{J_{ac}L_{equ}}.$$

Where, A is the system matrix; B is the input matrix; C is the output matrix, and D is the direct-feed through matrix; x is the state variable; θ_{ac}^* is the reference input; $e = \theta_{ac}^* - \theta_{ac}$ is the tracking error; u is the control input; w is the disturbance input; y is the output variable.

In view of the fact that reference input does not affect the procedure of controller design, assuming input of the system is zero for the convenience of controller design. Thus, the tracking error e has the form

$$e = -\theta_{ac} = -y \quad (24)$$

Let $x_k = \int y dt$, $\dot{x}_k = y$, the control input u is

$$u = -K_p Cx - K_i x_k - K_d C\dot{x} \quad (25)$$

Then, the control problem of the closed-system is equivalent to the problem of parameter determination for robust PID controller. $K = [K_p, K_i, K_d]$, for a real scalar such that $\gamma > 0$, and the transfer function $H(s)$ from disturbance w to the controlled output must satisfy the following H^∞ norm constrained control

$$\|H(s)\|_\infty < \gamma \quad (26)$$

Define $\hat{x} = (x, x_k)^T$, and then state space realization of the closed-loop augmented system for system (23) can be expressed as[13]

$$\begin{cases} \dot{\hat{x}} = (\bar{A} - \bar{B}K\bar{C})\hat{x} + \bar{B}w \\ y = \hat{C}\hat{x} \end{cases} \quad (27)$$

Here,

$$\begin{aligned}\bar{A} &= \begin{bmatrix} A & 0 \\ C & 0 \end{bmatrix}; \\ \bar{B} &= \begin{bmatrix} B \\ 0 \end{bmatrix}; \\ \hat{C} &= [C \ 0]; \\ \bar{C} &= \begin{bmatrix} 0 & 0 & 1 & 0 \\ 0 & 0 & 0 & 0 \\ 0 & 1 & -a_{33} & 0 \end{bmatrix}.\end{aligned}$$

Given a real scalar γ , then the necessary and sufficient condition for the asymptotic stability of the closed-loop system (27), as well as satisfying (26) is equivalent to the existence of a positive definite symmetric matrices P , which is the solution of the following inequality

$$\begin{aligned}(\bar{A} - \bar{B}K\bar{C})P + P(\bar{A} - \bar{B}K\bar{C})^T \\ + \gamma^{-2}P\hat{C}^T\hat{C}P + \bar{B}\bar{B}^T < 0\end{aligned}\quad (28)$$

According to the Schur complement theory, equation (28) can be rewritten as

$$\begin{bmatrix} \psi & P\hat{C}^T \\ \hat{C}P & -\gamma^{-2}I \end{bmatrix} < 0\quad (29)$$

Where,

$$\psi = (\bar{A} - \bar{B}K\bar{C})P + P(\bar{A} - \bar{B}K\bar{C})^T + \bar{B}\bar{B}^T.$$

For equation (29) contains nonlinear terms, replacement of variable matrix must be conducted, and denote $S = K\bar{C}P$, as well as define

$$\begin{aligned}S &= \begin{bmatrix} 0 & S' \end{bmatrix} \in \mathbb{R}^{1 \times 4}, \quad S' \in \mathbb{R}^{1 \times 3} \\ P &= \begin{bmatrix} P_{11} & 0 \\ 0 & P_{22} \end{bmatrix} \in \mathbb{R}^{4 \times 4}, \quad P_{11} \in \mathbb{R}^{1 \times 1}, P_{22} \in \mathbb{R}^{3 \times 3}\end{aligned}\quad (30)$$

Thereupon, solving problem for the Robust PID controller K is equivalent to the existence of matrix variable $[S', P_{11}, P_{22}]$ satisfying

$$\begin{bmatrix} AP - \bar{B}S + P\bar{A}^T - S^T\bar{B}^T + \bar{B}\bar{B}^T & P\hat{C}^T \\ \hat{C}P & -\gamma^{-2}I \end{bmatrix} < 0\quad (31)$$

Then, parameters of the angular displacement controller K are

$$K = S'P_{22}^{-1}C_1^{-1}\quad (32)$$

Here,

$$C_1 = \begin{bmatrix} 0 & 1 & 0 \\ 0 & 0 & 1 \\ 1 & -a_{33} & 0 \end{bmatrix}$$

By using the function and calculator provided by LMI toolbox, parameters of the angular displacement controller can be solved.

3.2 Decision Control of Yaw Rate

In light of existing research results, reference values of yaw rate and side slip angle can be calculated by the following first order delay model [4][14]

$$\dot{x}_d = A_d x_d + B_d u_d\quad (33)$$

Where, μ_0 is referred to as the reference value of road adhesion coefficient, $x_d = [r_d, \beta_d]^T$ is the state, $u_d = \theta_p'$ is the input,

$$\begin{aligned}A_d &= \begin{bmatrix} -\frac{1}{\tau_r} & 0 \\ 0 & 0 \end{bmatrix}; \\ B_d &= \frac{1}{G} \begin{bmatrix} \frac{a_r}{\tau_r} \\ 0 \end{bmatrix}; \\ \tau_r &= \frac{I_z V}{K_f \mu_0 l_f L + m l_f V^2}; \\ a_r &= \frac{\mu_0 K_f V l_f L}{\mu_0 K_f l_f^2 L + m l_f l_r V^2}.\end{aligned}$$

The main objective for yaw rate control is to reduce the response delay of vehicle driving on the road with low adhesion coefficient, thus to make the response characteristics of vehicle close to that on the road with good adhesion coefficient, reference value of road adhesion coefficient μ_0 was chosen as 0.85.

Define e_r is the error between reference and real values of yaw rate, and e_β is the error between reference and real values of side slip angle. Then, e_r and e_β can be obtained by following function

$$e_{sta} = \begin{bmatrix} e_r \\ e_\beta \end{bmatrix} = \begin{bmatrix} r_d - r \\ \beta_d - \beta \end{bmatrix} = x_d - \hat{x}\quad (34)$$

Yaw rate control was conducted based on the feedback of yaw rate and side slip angle together, as well as control law u_{sta} can be described as

$$\begin{aligned}u_{sta} &= \frac{1}{G} \theta_p' + K_{sr} (r_d - r) + K_{s\beta} (\beta_d - \beta) \\ &= \frac{1}{G} \theta_p' + [K_{sr}, K_{s\beta}] \begin{bmatrix} r_d - r \\ \beta_d - \beta \end{bmatrix}\end{aligned}\quad (35)$$

Let $K_{sta} = [K_{sr}, K_{s\beta}]$, then the control law described in equation (35) can be rewritten as

$$u_{sta} = \frac{1}{G} \theta_p' + K_{sta} e_{sta} \quad (36)$$

For θ_p' is applied by driver and active steering control together, thus assuming $\theta_p' = 0$ in the control law u_{sta} described in equation (36), which does not affect the design of the yaw rate controller. Thus, the control law u_{sta} has the following form

$$u_{sta} = K_{sta} e_{sta} \quad (37)$$

To study the optimal control problem, performance index of linear quadratic regulator (LQR) was introduced and described by[15]

$$J = \frac{1}{2} \int_0^\infty (e_{sta}^T Q e_{sta} + u_{sta}^T R u_{sta}) dt \quad (38)$$

Here, Q and R are weighting matrices, $Q \in R^{2 \times 2}$ is positive semidefinite matrix, $R \in R^{1 \times 1}$ is positive definite matrix, and the method to choose parameters of weighting matrices Q and R was shown in reference[16]. In the performance index of equation (38), $e_{sta}^T Q e_{sta}$ can be used to measure the comprehensive error between the reference and real values during the whole control period, and $u_{sta}^T R u_{sta}$ used to limit the control energy.

The first-order derivative of the errors e_r and e_β can be given by

$$\begin{aligned} \dot{e}_{sta} &= \begin{bmatrix} \dot{e}_r \\ \dot{e}_\beta \end{bmatrix} = \dot{x}_d - \dot{\hat{x}} = A_d x_d + B_d u_d - \hat{A} \hat{x} - \hat{B} u_{sta} \\ &= \hat{A} x_d - \hat{A} \hat{x} + A_d x_d - \hat{A} x_d + B_d u_d - \hat{B} u_{sta} \\ &= \hat{A} e_{sta} + (A_d - \hat{A}) x_d + B_d u_d - \hat{B} u_{sta} \end{aligned} \quad (39)$$

Then, variation method was adopted to solve the problem of linear quadratic optimal control, and the following hamiltonian function can be given by

$$\begin{aligned} H &= \frac{1}{2} e_{sta}^T Q e_{sta} + \frac{1}{2} u_{sta}^T R u_{sta} \\ &+ \lambda^T \left[\hat{A} e_{sta} + (A_d - \hat{A}) x_d + B_d u_d - \hat{B} u_{sta} \right] \end{aligned} \quad (40)$$

Here, $\lambda(t)$ is the lagrange multiplier vector.

Thus, control equation can be expressed as

$$\frac{\partial H}{\partial u_{sta}} = R u_{sta} + \hat{B} \lambda(t) = 0 \quad (41)$$

that is

$$u_{sta} = R^{-1} \hat{B}^T \lambda(t) \quad (42)$$

and adjoint equation is given by

$$-\frac{\partial H}{\partial e_{sta}} = \dot{\lambda}(t) = -Q e_{sta} - \hat{A}^T \lambda(t) \quad (43)$$

denote

$$\lambda(t) = P(t) e_{sta} \quad (44)$$

Then, first-order derivative of $\lambda(t)$ is defined as

$$\dot{\lambda}(t) = \dot{P}(t) e_{sta}(t) + P(t) \dot{e}_{sta}(t) \quad (45)$$

Let equation (43) equals equation (45), combine equations (39) and (44), as well as \hat{A} 、 \hat{B} 、 Q and R are constant matrices. With $t \rightarrow \infty$ and $\dot{P}(t) = 0$, the algebraic Riccati equation can be defined as follows

$$Q + P \hat{A} + \hat{A}^T P - P \hat{B} R^{-1} \hat{B}^T P = 0 \quad (46)$$

Parameters of matrix P can be obtained by solving equation (46), then parameters of the optimal controller can be calculated by the following equation

$$K_{sta} = R^{-1} \hat{B}^T P \quad (47)$$

According to the parameters of active steering actuator, additional angle θ_{ac}^* conducted by yaw rate control is

$$\theta_{ac}^* = G K_{sta} e_{sta} \quad (48)$$

4 Numerical Simulation

To verify the control effectiveness of the double closed-loop control scheme, a serious numerical simulation of limiting conditions were carried out. Referencing the limiting conditions adopted by existing literatures, with or without disturbance of side wind on ice-snow road condition was used as limiting conditions. Performance of the double closed-loop control scheme of yaw rate was verified from two aspects: decrease of response delay for vehicle driving on the road with low adhesion coefficient, as well as inhibition effects of unexpected yaw disturbance on the response characteristics of vehicle.

4.1 Limiting Condition I

In limiting condition I, road adhesion coefficient and vehicle velocity were chosen as 0.2 and 80Km/h respectively. Sinusoidal input was used as steering wheel angle, which amplitude and frequency were chosen as 3 degree and 0.1Hz respectively. Simulation results of yaw rate in limiting condition I are shown in Fig.5.

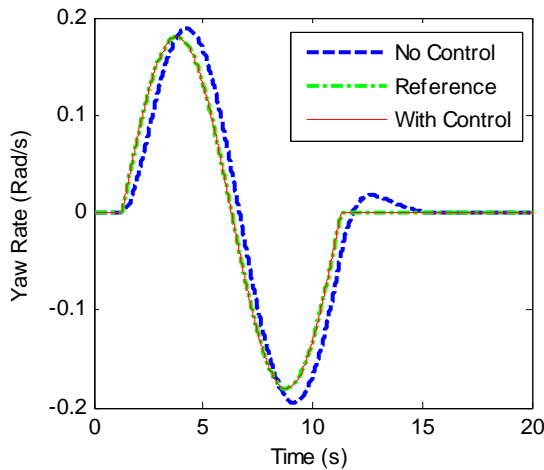


Fig.5 Results of yaw rate in limiting condition I

As shown in Fig.5, response delay of yaw rate is serious without yaw rate control. By double closed-loop control for yaw rate, vehicle yaw rate can track the reference value of yaw rate very well. In addition, response delay of vehicle driving on the road with low adhesion coefficient can be reduced, so the control effect is good.

4.2 Limiting Condition II

Limiting condition II was based on the limiting condition I, and disturbance of side wind was applied. The speed model of side wind proposed by National Aeronautics and Space Administration (NASA) was adapted to simulate driving environment with the effect of side wind. The speed of the side wind and force conducted by side wind are shown in Fig.6 and Fig.7 respectively. Simulation results of yaw rate in limiting condition II are shown in Fig.8.

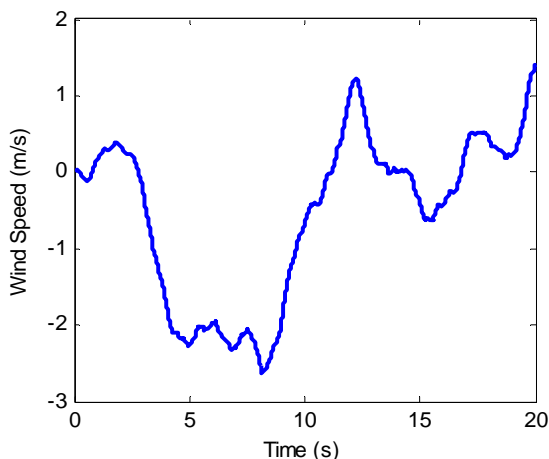


Fig.6 Side wind speed

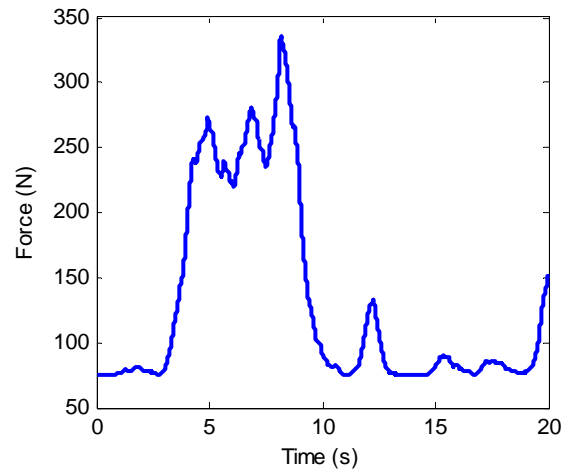


Fig.7 The force conducted by side wind

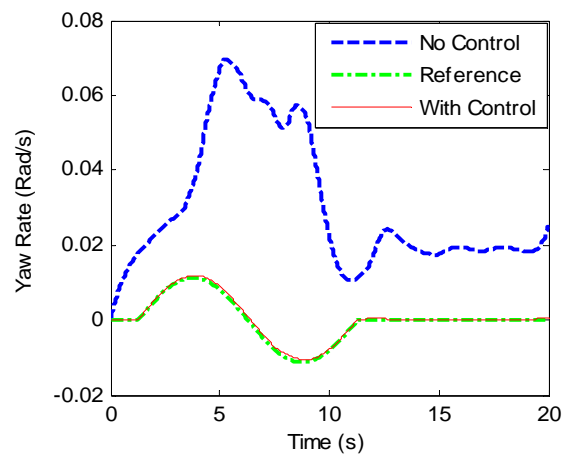


Fig.8 Results of yaw rate in limiting condition II

Compared with Fig.5, it can be inferred from Fig.8 that amplitude of yaw rate is increased with the disturbance of side wind, that is to say, a greater yaw disturbance was produced. By double closed-loop control for yaw rate, vehicle yaw rate can still track the reference value of yaw rate very well, and the tracking error is small, which means that the lateral stability can be improved.

Thus, effects of unexpected yaw disturbance on the response characteristics of vehicle can be weakened effectively.

5 Virtual Test in Limiting Conditions

To further validate the effectiveness of the double closed-loop control scheme of yaw rate, virtual test of limiting condition I and II were conducted based on CarSim software. Extended Simulink function of CarSim was used to construct co-simulation model between CarSim and Simulink, detailed modeling process can be described as follows.

Firstly, characteristic parameters of main part for whole vehicle was set in the main screen of the CarSim software, as well as terrain characteristics of virtual road was set in the module of “Test Specifications”. Performance parameters of whole vehicle can be set in the module of “Vehicle ConFig.uration”, in which car body model was selected as “Sprung mass (whole)”. Meanwhile, road adhesion coefficient can be set in the sub module of “Proceduce”.

Secondly, steering system was set for “Steering (Simple)”, as well as the double closed-loop control scheme of yaw rate and speed model of side wind were created in the platform of Simulink. Meanwhile, characteristic parameters of the steering system could be adjusted accordingly.

Thirdly, in the module of “Miscellaneous Data” for the main screen of CarSim software, control characteristics of speed can be set as “Control:

Speed (Closed Loop) VS. Time”, then the constant speed condition can be realized by this control mode.

Finally, running mode was selected as “Run Control with Simulink” in the main screen of the CarSim software, as well as input and output signals were set in the screen of “I/O Channels”. Here, yaw rate, side slip angle and speed were set as output signals, while steering wheel angle and force conducted by side wind were set as input signals. Meanwhile, active mode for the input signals was selected as “Replace”.

Then, construction of co-simulation communication interface between CarSim and Simulink was completed, and the co-simulation communication interface was shown in Fig.9.

The two kinds of limiting conditions were applied to the virtual tests based on CarSim, and results of the virtual tests in limiting condition I and II are shown in Fig.10 and Fig.11 respectively.

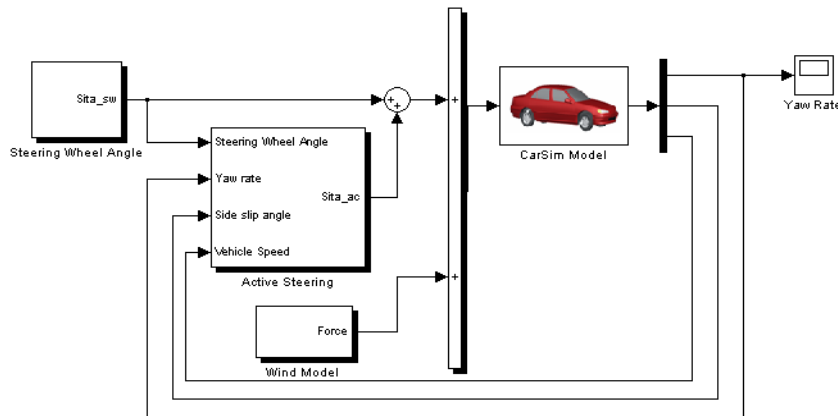


Fig.9 Co-simulation communication interface between CarSim and Simulink

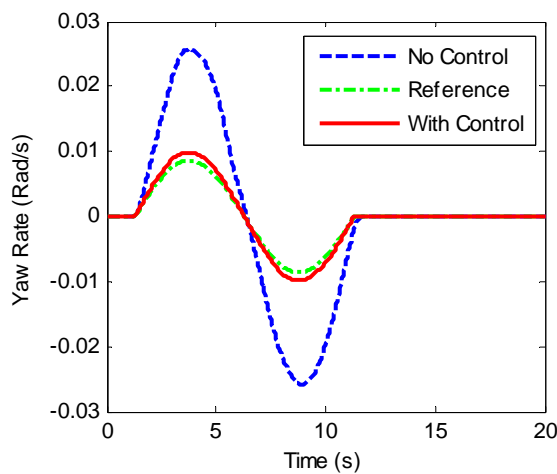


Fig.10 Virtual test results of yaw rate in limiting condition I

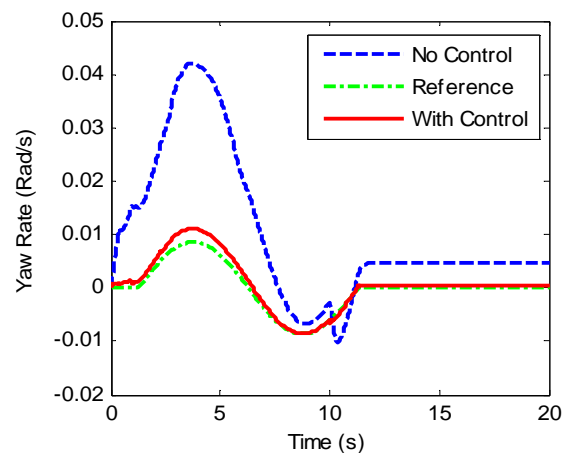


Fig.11 Virtual test results of yaw rate in limiting condition II

As shown in Fig.10, by double closed-loop control for yaw rate, vehicle yaw rate can track the reference value of yaw rate very well, which means that response delay of vehicle driving on the road with low adhesion coefficient can be reduced, as noted in the numerical simulation study of the limiting condition I.

It is obvious from the Fig.11 that effects of unexpected yaw disturbance on the response characteristics of vehicle can be weakened effectively, as is pointed out in the numerical simulation study of the limiting condition II.

The above results suggest the view that the effectiveness and robustness of the double closed-loop control scheme of yaw rate is good. This also proves the results obtained in the former numerical simulation study.

6 Conclusion

To improve the control accuracy of the actuator motor for active front steering, a double closed-loop control scheme of yaw rate for active front steering was proposed, and a serious numerical simulation of limiting conditions were conducted. To further validate the effectiveness of the double closed-loop control scheme of yaw rate, virtual tests of limiting conditions were carried out based on CarSim software. Numerical simulation and virtual test results indicate that response delay of vehicle driving on the road with low adhesion coefficient can be reduced by double closed-loop control of yaw rate, and effects of unexpected yaw disturbance on the response characteristics of vehicle can be weakened effectively. Thus, the effectiveness and robustness of the double closed-loop control scheme of yaw rate is good.

References:

- [1] W. A. H. Oraby, S. M. El-Demerdash, A. M. Selim, A. Faizz, and D. A. Crolla, Improvement of Vehicle Lateral Dynamics by Active Front Steering Control, *SAE Technical Paper Series*, USA:SAE Publication Group, Paper Number: 2004-01-2081.
- [2] Choi Ju Yong, Kim Chang-Sup, Hong, Sinpyo Pyo, et al., Vision Based Lateral Control by Yaw Rate Feedback, *Proceedings of 27th Annual Conference of the IEEE Industrial Electronics Society*, Vol.3, 2001, pp. 2135-2138.
- [3] Zheng, Bing ; Oh, Pahngroc ; Lenart, Bany, Active Steering Control with Front Wheel Steering Proceedings of the 2004 American Control Conference, Vol.2, 2004, pp. 1475-1480.
- [4] Li Qiang, Shi Guobiao, Lin Yi, and Wei Jie, Yaw Rate Control of Active Front Steering based on Fuzzy-Logic Controller, *Proceedings of 2010 Second International Workshop on Education Technology and Computer Science*, Vol.1, 2010, pp.125-128.
- [5] B A Güvenç, L Güvenç, D Odenthal, et al. Robust Two Degree of Freedom Vehicle Steering Control Satisfying Mixed Sensitivity Constraint, *Proceedings of the European Control Conference*, 2001, pp. 1198-1203.
- [6] S Mammam, V B Baghdassarian, Two-Degree-of-Freedom Formulation of Vehicle Handling Improvement by Active Steering, *Proceedings of American Control Conference (ACC)*, USA: IEEE, Vol. 1, No.6, 2000, pp. 105-109.
- [7] A S O Al-Mashakbeh, Proportional Integral and Derivative Control of Brushless DC Motor, *European Journal of Scientific Research*, Vol. 35, No.2, 2009, pp. 198-203.
- [8] Ji Zhi-cheng, SHEN Yan-xia1, JIANG Jian-guo1, A Novel Method for Modeling and Simulation of BLDC System Based on Matlab, *Acta Simulata Systematica Sinica*, Vol.15, No.12, 2003, pp.1745-1758.
- [9] G R Yu, R C Hwang, Optimal PID Speed Control of Brushless DC Motors Using LQR Approach, *Proceedings of the IEEE International Conference on Systems, Man and Cybernetics*, USA: IEEE, 2004: 473-478.
- [10] M K Salaani, G J Heydinger, P A Grygier, Vehicle On-Center Directional and Steering Sensitivity, *SAE Technical Paper Series*. USA: SAE Publication Group, Paper Number: 2005-01-0395.
- [11] W Gawronski, J Mellstrom, Field Verification of the Wind Tunnel Coefficients, *The Telecommunications and Data Acquisition Progress Report 42-119*, 1994, pp. 210-220.
- [12] F Momiyama, E Kitagishi, N Tokuda, Electro-Hydraulic Feedforward Control Power Steering System for Trucks and Buses, *SAE Technical Paper Series*, USA: SAE Publication Group, Paper Number: 892519.
- [13] Li Huijun, Chen Mingjun, Design of H_∞ Robust PID Controller Based on LMI, *Control Engineering of China*, Vol. 14, No.3, 2007, pp. 294-296.
- [14] M Nagai, S Yamanaka, Y Hirano, "Integrated Control of Active Rear Wheel Steering and Yaw Moment Control Using Braking Forces,"

JSME International Journal, Series C, Vol. 42, No.2, 1999, pp. 301-308.

- [15] Hu Shousong, Wang Zhiquan, Hu Weili, *Optimal Control Theory and System*, 2nd ed., Beijing: Clarendon, 2005, pp. 212-222.
- [16] Du feng, Li Lun, Wei Lang, Zhao Jianyou, *Optimal Control for Active 4WS Vehicle Based on Model Tracking Technology*, *Tractor & Farm Transporter*, vol. 36, No.1, 2009, pp 16-18.

Acknowledgement

This work was supported by National Natural Science Foundation of China (Grant No.51375007), and this program was supported by Ningbo Natural Science Foundation (Grant No. 2013A610151).